Specific *OCRL1* patient mutations differentially impact Lowe Syndrome cellular phenotypes

Swetha Ramadesikan[1‡], Lisette Skiba[1], Jennifer Lee[1], Kayalvizhi Madhivanan[1¶], Daipayan Sarkar[1], Agustina De La Fuente[1], Claudia B. Hanna[1] Tony Hazbun[2], Daisuke Kihara[1,3] and R. Claudio Aguilar[§1]

1. Department of Biological Sciences, Purdue University, West Lafayette, IN 47907.

2. Department of Medicinal Chemistry and Molecular Pharmacology, Purdue University, West Lafayette, IN 47907.

3. Department of Computer Science, Purdue University, West Lafayette, IN 47907.

‡: Current address: Institute for Genomic Medicine, Nationwide Children's Hospital, Columbus OH 43205

¶: Current address: Department of Pathology and Neuroscience, University of California- San Diego, La Jolla, CA 92093.

§: Corresponding author: Phone: 1-765-496-3547; e-mail: claudio@purdue.edu

Keywords: Lowe syndrome, *OCRL1* mutations, inositol 5' phosphatase, Golgi fragmentation, conformational disease.

ABSTRACT

Lowe Syndrome (LS) is a lethal genetic disorder caused by mutations in the *OCRL1* gene, which encodes the lipid 5' phosphatase Ocrl1. Patients exhibit a characteristic triad of symptoms including eyes, brain and kidneys abnormalities with renal failure as the most common cause of death. Over 200 *OCRL1* mutations have been identified in LS, but their specific impact on cellular processes is unknown. Despite observations of heterogeneity in LS patient symptoms, there is little understanding of the correlation between the genotype of patients and disease and/or cellular phenotypes.

Here, we showed that different mutations had diverse effects on protein localization, stability and on triggering LS cellular phenotypes. In addition, mutations in specific domains imparted unique characteristics to the resulting mutated protein. We also propose that some mutations conformationally affect the 5'-phosphatase domain of the protein, resulting in additional phenotypes and loss of activity.

This study is the first to show the differential effect of patient 5'-phosphatase mutations on cellular phenotypes and introduces a conformational disease component in LS. This work can provide a framework that can help stratify patients as well as provide a more accurate prognosis depending on the nature and location of the mutation in the *OCRL1* gene and its effect on the biochemical activity of Ocrl1.

INTRODUCTION

Lowe Syndrome (LS) (OMIM#30900) is an X-linked genetic disorder caused by mutations in the *OCRL1* gene (1). Affected children suffering from the disease are born with bilateral congenital cataracts and develop neurological and renal symptoms as early as 6 months of age (2, 3). Progressive renal dysfunction leads to end stage renal disease and their premature death (2), and unfortunately there are currently no LS-specific therapeutics (4).

The gene product of *OCRL1* is an inositol 5' phosphatase (EC 3.1.3.36) (5, 6) called Ocrl1. Ocrl1 localizes at the *trans*-Golgi network (TGN) (7), endosomes (8) and transiently at the plasma membrane (9). The lipid phosphatase has specificity for the signaling lipid phosphatidyl inositol 4,5-bisphophate, PI(4,5)P_2 (5, 6). In addition to its phosphatase domain, Ocrl1 possesses an N-terminal PH domain (10) and C-terminal ASH-RhoGAP (8, 11) domains through which it interacts with several signaling and trafficking proteins in cells, thereby participating in several basic cellular processes including cell migration, cell spreading, actin remodeling, ciliogenesis, vesicle trafficking, cytokinesis and phagocytosis (12-22). Further, we determined that Ocrl1 participates in the above two processes is through determinants spatially segregated within the protein (with the N-terminus required for membrane remodeling (12) and the C-terminus required for primary cilia assembly (15)); while a functional Ocrl1 5'-phosphatase domain is required for both processes to proceed normally (12, 15).

There are over 200 unique LS-causing mutations that have been identified in *OCRL1* (4, 23) and affect all domains of Ocrl1.

Therefore, it could be expected that mutations differentially affecting various regions of Ocrl, would have different impact on cellular phenotypes causing heterogeneity in LS patient

symptoms (4, 23); however, little is known about the correlation between the genotype of patients (involving over 200 unique *OCRL1* mutations) and their cellular phenotypes.

Here we show that depending on the domain they affect, different *OCRL1* mutations have a differential impact on cell spreading and ciliogenesis, thereby proposing cellular basis for LS patient symptom heterogeneity. In addition, specific mutants possess unique characteristics in terms of localization and protein stability. Importantly, some of the phosphatase domain mutants tested produced fragmentation of the Golgi apparatus, a phenotype exclusive to this domain. This novel cellular phenotype has been associated with neurodegenerative diseases (24-26). Given that LS has a neurological component, we predict that this defect may play a role is disease pathogenesis.

In addition, molecular dynamics analysis of Ocrl1 patient variants with residue changes at non-catalytic sites of the phosphatase domain predicted the existence of conformational changes affecting the enzyme active site. Indeed, experimental results showed impairment of 5'-phosphatase activity for these mutants as well as the presence of cellular phenotypes in cells expressing these variants. These results not only explain how mutations affecting non-catalytic residues cause LS but also imply that some *OCRL1* mutants lead to a conformational/protein misfolding disease scenario.

In summary, our results provide the first comprehensive analysis of the effect *OCRL1* mutations on cellular phenotypes likely to impact overall embryogenesis and organ-specific function (*e.g.,* kidneys). Our data also establishes a conformational disease component for some Lowe Syndrome patients. We believe that this study will provide the framework that can stratify LS patients as well as allow aid in creating tailored therapeutic strategies that would consider the

nature, location of mutation in the gene and its effect on the biochemical activity and protein domains of Ocrl1.

RESULTS

Ocrl1 patient variants selected for this study

This study is focused on understanding the consequences of *OCRL1* misense mutations on several characteristics (stability, localization and ability to sustain specific cellular functions) of the encoded 5'-phosphatase Ocrl1.

Since 90% of missense mutations found in LS patients locate within *OCRL1*'s exons encoding for the enzyme phosphatase domain and its ASH (ASPM-SPD-2-Hydin)-RhoGAP (RhoGTPase Activating Protein) regions (4, 23, 27), for this study we selected patient missense mutations located within exons 9-23 (Table I and Fig. 1A)

Specifically, there are nearly 80 unique missense LS-causing mutations which lead to amino acid changes affecting the Ocrl1's phosphatase domain. While many of these replacements map to conserved regions important for catalysis and substrate recognition, others affected residues not directly involved in substrate binding and processing. Therefore, we selected Ocrl1 patient variants to represent both categories; *i.e.,* H524R (critical catalytic residue replaced), S256N, D451G and V508D (affecting non-catalytic residues). There are nearly 20 unique missense mutations resulting in changes in the amino acids encoding the C-terminal ASH-RhoGAP domain of Ocrl1. From these, we selected variants V577E, F668V and I768N.

Although a few variants with amino acid changes have been found in Ocrl1's PH domains, there are no reported LS-causing missense mutations in exons 2-7. Nevertheless, several nonsense, frameshift mutations and deletions have been found within these 5' exons of the *OCRL1* gene which cause LS or a milder form known as Dent-2 disease (27). Interestingly, Shrimpton et al. (28) proposed that in these cases an alternative initiation codon (corresponding to Ocrl1's Met187)

is used to translate an N-terminal truncation (lacking the PH domain) that would retain substantial functionality. We recreated such Ocrl1$^{187-901}$ (ΔPH) product for characterization in this study (Fig.1B).

Ocrl1 patient variants differentially affect cell spreading and ciliogenesis in human kidney epithelial cells

Since renal failure is the main cause of death among LS patients, in this study we used human embryonic kidney 293T (HEK293T) epithelial cells lacking *OCRL1* (HEK293T KO) and focused on cell spreading and ciliogenesis as cellular readouts.

Cell spreading: We transfected the different GFP-tagged Ocrl1 mutated variants or Ocrl1^{WT} in HEK293T KO cells and performed standard spreading assays as described before (12) and in *Materials and Methods*. Briefly, 18h after transfection, cells were lifted and allowed to attach and spread for 30min on fibronectin-coated coverslips. After 30min of attachment and spreading, cells were fixed with 4% formaldehyde, stained with rhodamine-phalloidin to label the actin cytoskeleton. Random fields containing transfected cells were imaged and spreading area was measured using magic wand tracing tool in ImageJ and statistical analysis were performed as described in *Materials and Methods*.

In agreement with the hypothesis that Ocrl1's N-terminus region is required for membrane remodeling (12), Ocrl1$^{\Delta PH}$ showed a spreading defect (Fig 2A).

We also found that cells expressing any Ocrl1 patient variant bearing a mutated phosphatase domain displayed significant smaller spreading areas compared to those expressing Ocrl1^{WT} (Fig.2B). Nevertheless, specific mutants induced different degree of severity in the cell spreading

phenotype; *e.g.,* while Ocrl1^{V508D} was only modestly affected (~12% reduction in median spreading area compared to WT), Ocrl1^{D451G} and Ocrl1^{H524R} showed a more severe spreading phenotype (Fig.2B). Interestingly, Ocrl1^{S256N} did not induce a striking spreading defect in cells (Fig.2B).

In contrast and although cells expressing ASH-RhoGAP mutants Ocrl1^{V577E},Ocrl1^{F668V},Ocrl1^{I768N} were prone to show smaller cell spreading area, the differences were not statistically significant as compared to WT (Fig.2C). These results were in agreement with previous observations that the C-terminal region of Ocrl1 was not critical for membrane remodeling (12).

Ciliogenesis: We also tested the impact of Ocrl1 patient mutated variants on primary cilia (PC) assembly in HEK293T KO cells. Cells were seeded at ~30-50% confluency, transfected with plasmids for expression of Ocrl1 patient variants and ciliogenesis assays were performed as described previously (15) and in *Materials and Methods*. Briefly, 18h after transfection, cells were starved for 24h by maintaining them in 0.1% FBS media to induce ciliogenesis. After that, cells were fixed with 4% formaldehyde, followed by indirect immunofluorescence using antibodies against acetylated tubulin (to label primary cilia) and pericentrin-2 (to label centriole; base of cilia). Fields were randomly imaged and the fraction of Ocrl1 mutant transfected cells forming a cilium was calculated and compared to the fraction of ciliated Ocrl1^{WT}-expressing cells (See *Materials and Methods*).

Interestingly, Ocrl1$^{\Delta PH}$ was unaffected for ciliogenesis (Fig.3A), likely due to the presence of functional phosphatase and ASH-RhoGAP domains which were previously shown by our lab to be required for PC assembly (15). These results also suggested that the N-terminal truncated

Ocrl1 variant starting at M187 is partially functional as it was capable of sustain ciliogenesis, although it lacked the ability to facilitate cell spreading.

All cells expressing phosphatase mutants were affected for ciliogenesis in varying degrees (Fig.3A). Similar to their effect on the cell spreading, ciliogenesis phenotype severity varied among different patient variants. While presence of Ocrl1^{H524R}, Ocrl1^{S256N}, Ocrl1^{D451G} led to cells severely impaired for this PC assembly, expression of Ocrl1^{V508D} had a significant but milder phenotype.

Along the same lines, cells expressing the ASH-RhoGAP V577E, F668V and I768N mutated variants were also differentially affected for ciliogenesis as compared to Ocrl1^{WT} (Fig.3B).

Cellular phenotypes and protein localization abnormalities associated with specific Ocrl1 patient mutated variants

In addition to well-established LS cellular phenotypes such as defects in membrane remodeling (e.g., cell spreading) and ciliogenesis, certain patient mutated variants exhibited the following specific phenotypes and/or localization abnormalities: a) *Ocrl1$^{\Delta PH}$ deficient localization;* b) *Induction of Golgi apparatus fragmentation* by some Ocrl1 patient variants bearing mutated phosphatase domain (these variants also showed a disperse punctate pattern with poor TGN co-localization). c) *Mislocalization to centriolar structures* in Ocrl1 variants bearing mutated ASH-RhoGAP domain (some of these variants also exhibited cytosolic aggregates).

a) *Ocrl1$^{\Delta PH}$ deficient localization:* GFP-Ocrl1$^{\Delta PH}$ localized to the TGN like Ocrl1^{WT}, but surprisingly, it was more cytosolic and enriched in the nucleus (Fig.4). Since it is well-known that GFP has non-specific affinity for the nucleus (top left panel Fig.4), we speculate that lack of

the PH domain makes Ocrl1 more susceptible to be dragged into the nucleus by fusion to GFP. Therefore, this aberrant mis-localization of the Ocrl1$^{\Delta PH}$ variant to the nucleus suggests that the N-terminal contributes to maintain proper Ocrl1's intracellular localization.

b) *Induction of Golgi apparatus (GA) fragmentation*: We had previously observed that overexpression of the patient's phosphatase-dead Ocrl1^{H524R} variant led to fragmentation of the Golgi complex in HeLa cells (12). Along the same lines, it has been also reported that an artificial Ocrl1 truncated construction lacking the phosphatase domain induced a similar phenotype (16). It should be highlighted that GA fragmentation has been associated with neurological disorders including Alzheimer's disease, Parkinson's disease, Huntington's disease, amyotropic lateral sclerosis (ALS), Angelman syndrome, spinal muscular atrophy and epilepsy (24-26, 29, 30). Given the presence of a neurological component in LS (2, 4), we speculate that this cellular phenotype is relevant to disease pathogenesis.

Since our previous results linked mutations affecting the 5'-phosphatase domain in Ocrl1 patient variants we tested their ability to induce GA fragmentation (measure as the ratio between the GA and the whole cell area, see *Materials and Methods*—Fig. 5A,B) in HK2 *OCRL1* K.O. (HK2 KO) cells. HK2 cells are larger in size and possess a flatter morphology than HEK293T, making them more suitable to microscopy analysis (in addition, all phenotypes described before for each Ocrl1 mutated variant were also observed in in HK2 KO cells; data not shown).

While HK2 KO cells expressing Ocrl1^{WT} showed a continuous and compact Golgi complex, as seen by labeling the *trans*-Golgi network (using an anti-TGN46 antibody) and the *cis*-Golgi network (using an anti-GM130 antibody), cells expressing patient variants D451G and V508D displayed a discontinuous and fragmented Golgi complex that occupied a larger cellular area than

the one covered by the GA in cells expressing Ocrl1^{WT} (Fig.5A, second and third panel). Interestingly, we also observed that these Ocrl1 mutated variants displayed a dispersed punctate pattern themselves (Fig. 5A) with poor colocalization between the mutated Ocrl1 variant and TGN46 or GM130 (Fig. 5A, inset- arrows (mutant Ocrl1) and arrowheads (TGN)). In contrast, cells expressing Ocrl1^{S256N} did not show GA fragmentation (Fig. 5A, bottom most panel).

Importantly, the magnitude of the GA fragmentation was independent of the amount of GFP-tagged Ocrl1 mutated variant expressed (measured as total cell-associated green fluorescence intensity, Fig. 5C). Along the same lines, this phenotype was also observed in HK2 KO cells stably expressing the 5'-phosphatase affected Ocrl1^{H524R} variant (Fig. 5D&E). Similar results were observed using HeLa and HEK293T cells (Data not shown).

In summary, although Golgi apparatus fragmentation in untransfected HK2 KO cells was barely detectable, three of the four different phosphatase domain missense mutations, when expressed transiently or stably in cells lacking Ocrl1 induced Golgi apparatus fragmentation. *This also suggests that presence of some mutants may induce phenotypes that may be more severe than those produced when Ocrl1 is absent.*

c) *Mislocalization to centriolar structures*: Transient expression of GFP-tagged ASH-RhoGAP mutants Ocrl1^{V577E}, Ocrl1^{F668V} and Ocrl1^{I768N} in HEK293T KO cells under steady state conditions displayed a characteristic perinuclear punctate structure (Fig.2C, yellow arrows). Same observations were made using HK2 KO cells (Fig.6A, yellow arrows & Ocrl1 panel inset).

Upon serum-starvation conditions (to induce PC assembly- (15), Ocrl1^{WT} has been shown to localize transiently at the base of the cilium (where the axoneme-linked centrioles localize), presumably for trafficking of ciliary cargo to the PC (15). Therefore, and *although steady state*

experiments are not done under serum-starvation conditions, we wondered if the punctate structure observed in cells expressing ASH-RhoGAP mutated Ocrl1 would colocalize with the centrioles. Indeed, we found that GFP-tagged Ocrl1^{V577E}, Ocrl1^{F668V} and Ocrl1^{I768N} perinuclear punctate structures colocalized with pericentrin-2 (PC2: a centriole marker, Fig. 6A&B). In fact, using serum-supplemented media, we could *not* observe Ocrl1^{WT} at the centriole at all.

In addition, ASH-RhoGAP mutated Ocrl1^{V577E}, Ocrl1^{F668V} and Ocrl1^{I768N} patient variants had an overall diffuse cytosolic appearance in cells and lacked typical perinuclear Golgi apparatus enrichment (Fig.6A). We also analyzed centriolar localization of the ASH-RhoGAP mutated proteins as function of their levels of expression. Specifically, we segregated transfected cells into 'low' (>80% of the total cell population), 'medium' and 'high' total fluorescence intensity (*i.e.,* total protein content) groups covering the entire population (Fig. 6C). Independently of the total fluorescence intensity, GFP-tagged Ocrl1 patient variants Ocrl1^{V577E}, Ocrl1^{F668V} and Ocrl1^{I768N} colocalized with the centriole (Fig. 6C). Further, at higher levels of expression, Ocrl1 mutated proteins Ocrl1^{V577E} and Ocrl1^{I768N} showed evidence of protein aggregation (Fig. 6D). Although this may not occur at physiological levels of expression, it suggested a destabilizing effect these ASH-RhoGAP mutations Ocrl1.

In addition, low copy number, stably-expressing Ocrl1^{I768N} cells also showed centriolar and diffuse cytosolic localization lacking TGN perinuclear enrichment typical of the WT protein (Fig.6E). In agreement with our observations on low-expressing transient transfectants, stably expressing cells did not exhibit protein aggregates (Fig. 6E).

Select *OCRL1* mutations affecting phosphatase domain likely cause a conformational change in catalytic domain of mutant protein

Although some of the tested Ocrl1 patient variants exhibited changes in phosphatase domain's residues not directly involved in binding/processing of substrate (Fig. 7A), they produced cellular defects linked to lack of enzymatic activity.

The phosphatase domain contains 6 conserved motifs essential for 5' phosphatase activity (31-34), as well as other conserved residues involved in substrate binding and lipid chain interactions (33, 35) (Fig.7A, yellow and grey highlighted regions). For example, the mutation H524R affects a critical residue that interacts with the scissile 5' phosphate (33, 35) (Fig.7A), and has been demonstrated to abolish phosphatase activity (36). In contrast, D451G and V508D affect residues that are found outside the conserved catalytic motifs within the phosphatase domain, and yet were affecting cellular functions of Ocrl1 (Fig.7A). We hypothesized that *these mutations affect the conformation of the catalytic domain, impairing its phosphatase activity.*

We used molecular dynamics (MD), to model residue changes D451G and V508D in the phosphatase domain of Ocrl1 (PDB ID: 4CMN). Our results predicted that although the changed amino acids were physically distant from the enzyme's active site, they induced conformation changes affecting critical catalytic residues (Fig.7B).

To determine if mutations D451G and V508D affected Ocrl1 phosphatase activity, we performed *in vitro* malachite green phosphatase assays (*Materials and Methods*) using bacterially purified GST-fusions of $Ocrl1^{1-563}$ (*i.e.,* truncations containing the PH-phosphatase domain) from patient variants (D451G, V508D and H524R) or WT.

As expected, $Ocrl1^{H524R}$ lacked phosphatase activity (Fig.8, top right panel). Importantly, and in agreement with our MD results, although the D451G and V508D amino-acid changes do not

directly affect the catalytic site of Ocrl1, they led to 5'-phosphatase domain inactivation (Fig.8 bottom left and right panels).

DISCUSSION

Complementing the pioneering works by different authors (12-16, 36-45) this study contributes to better understand Lowe syndrome as a complex disease. Here we highlight the heterogenous nature of this condition by focusing on the impact of different *OCRL1* mutations on typical LS cellular phenotypes while reporting new abnormalities triggered by specific patient variants. Indeed, this is the first systematic analysis of a selected group of mutations encoding for residue changes in all regions of Ocrl1.

On the one hand, data presented in this study supports the hypothesis that some Ocrl1's functional roles are segregated within the protein primary structure (12, 15, 42). Specifically, that integrity of the N-terminus being mostly required for membrane remodeling functions (e.g., cell spreading (12)), while Ocrl1's C-terminal region is relevant for ciliogenesis (15). As indicated before, the central phosphatase domain was required for both functions (12, 15). On the other hand, this study highlights specific phenotypes associated with certain mutations.

A predicted Ocrl1 patient variant that lacks its N-terminal PH domain but bears all other domains/regions should be therefore able to interact with Rab GTPases, required for proper intra-cellular localization (46-48). Indeed, similar to Ocrl1^{WT} this variant was enriched in compartments like the TGN; however, we still observed nuclear mis-localization. These observations suggest that absence of the PH domain led to the loss of previously unnoticed localization determinants, that allowed the GFP-tag to aberrantly drag/mislocalize the fusion protein to the nucleus. Nuclear localization is typical of free GFP (see Fig. 4 lower panel), but it is not observed in GFP-tagged Ocrl1^{WT} where the protein's strong localization determinants overpower the tag tendency to accumulate in the nucleus. Since Ocrl1$^{\Delta PH}$ lacks the N-terminal

region that contains one clathrin-binding motif (CBM) as well as the AP2-binding site (ABS), one could speculate of a possible role of clathrin and AP2 interactions for sustaining Ocrl1 proper localization. Alternatively, this may be revealing the presence of yet to be identified Ocrl1-interaction partners in the N-terminus that play a critical role in maintaining its cellular localization. This variant produced cellular phenotypes that were in agreement with the well demonstrated segregation of Ocrl1's functions across the protein domains, however we must consider if the mis-localization in any way contributed to some of the phenotypes in addition to the absence of the PH domain.

Specifically, we found that ASH-RhoGAP mutants were predominantly diffuse and cytosolic, lacking the Ocrl1^{WT}-like perinuclear enrichment. For these variants we also observed aggregates with dose-dependent abundance. Indeed, mutations affecting this domain are predicted to be destabilizing in nature, resulting in misfolded and/or degraded products (39, 49). Consequentially, this may either result in degradation or aggregation of mutant Ocrl1. Ultimately, if the protein gets eliminated or remains as aggregates, it will fail to be present where is needed (as observed by us), creating a scenario similar to having 'no Ocrl1'.

Presence of the ASH domain in different proteins is associated with localization at the centriole and cilia (11). Indeed, it is within this region that Ocrl1contains Rab-binding sites (46, 47) that during starvation (ciliogenesis-stimulating conditions) contribute to localization to and support the assembly of the primary cilia (15). However, Ocrl1 patient variants with their ASH-RhoGAP domains mutated localized at centriole even under steady state conditions (which was not the case for Ocrl1^{WT}). Importantly, this was observed even in a Rab-binding mutant

Ocrl1^{F668V} suggesting that this phenomenon is likely related to unique properties these mutants possess.

These mutants also produce aggregates at higher levels of expression. Though this may not necessarily be physiologically compatible, we observed a positive correlation in cells exhibiting aggregates and enrichment at centriole. Interestingly, subunits as well as substrates of proteosomal complexes have also been demonstrated to be enriched at the centriole (50). Given the proposed unstable nature of ASH-RhoGAP mutants, it is tempting to speculate that this enrichment is due to these misfolded or unstable proteins being targeted for degradation by the centriole-associated proteasome aka 'aggresome' (51-53). In fact, many other misfolded proteins implicated in diseases have been observed to be enriched in these compartments as well (51, 53).

It is of course possible that this aberrant enrichment may interfere with centriolar function. Centrioles are the microtubule organizing center; a nucleation site for primary cilia, facilitate cargo trafficking to the cilia and participate in cell division. Therefore, the likelihood of the Ocrl1 mutant accumulation contributing to the ciliogenesis defects observed with these variants cannot be ignored.

Several patient variants with mutated phosphatase domains (affecting either catalytic and non-catalytic) displayed a dispersed punctate pattern and induced Golgi apparatus fragmentation. Further, the Ocrl1 puncta mentioned above colocalized poorly with TGN. It should be noted that a similar phenotype has been observed in neurological diseases such as Alzheimer's disease, ALS, epilepsy, Huntington's disease (24-26), and therefore might be relevant for the neurological component of LS.

Besides Golgi apparatus fragmentation, these mutants produced substantial defects in cell spreading and ciliogenesis further supporting the idea that loss of enzymatic function affects both cellular processes. However, one of the most critical findings of this work is the conformational disease component of LS based on our analysis of the non-catalytic mutants Ocrl1^{D451G} and Ocrl1^{V508D}. This finding now allows us to understand and explain LS pathogenesis from the conformational disease point of view.

In fact, out of the 80 unique missense mutations within the phosphatase domain of Ocrl1, ~50% of the mutations (including D451G and V508D) are affecting non-catalytic residues and yet produce LS. We are actively pursuing studies to expand our understanding of whether these other non-catalytic mutations may behave in a similar manner.

In summary, our data shows that mutations have a diverse impact on protein stability as well as localization; which may produce a diverse range of cellular phenotypes, at times unique to specific domains. This generates a considerable degree of heterogeneity in LS cellular phenotypes.

Importantly, our findings also suggested that LS had a component of a 'conformational or misfolded protein disease'. A conformational disease is one where mutations in the gene lead to loss of function in the resultant mutant protein, either by affecting synthesis, transport stability, protein folding or its enzymatic activity (54) This causes the accumulation of the non-native conformation, rendering loss in function (54, 55). Infact, we mapped all known *OCRL1* missense mutations affecting the phosphatase domain and interestingly, found that ~50% of these mutations affect residues outside of the regions essential for catalysis within the domain.

Some well-studied conformational diseases include cystic fibrosis (54). In this disease, the gene *CFTR* (encoding a chloride channel) acquires a mutation that leads to the deletion of amino acid phenylalanine at position 508, resulting in CFTR ΔF508 mutant protein. This single mutation is found in almost 70% of the Caucasian patients (56), resulting misfolded mutant CFTR protein and subsequent accumulation in the endoplasmic reticulum (ER) As a result, this chloride channel protein does not localize to the cell surface, resulting in partial function, poor regulation of fluid composition in the airway. This produces thick mucus and respiratory difficulties in patients (56). Lowering the temperature (thermal stability) or treating with glycerol (a chemical chaperone) helped in releasing this mutant CFTR from the ER as well as restored its function (56).

Strikingly we observe that in some cases presence of a mutated Ocrl1 variant could be worse that the absence of this protein. Specifically, we found that some cellular phenotypes like Golgi apparatus fragmentation and cell spreading appear to be more severe in the presence of mutants $Ocrl1^{D451G}$ and $Ocrl1^{H524R}$ (independent of levels of expression) when compared to the complete absence of Ocrl1. One hypothesis to explain these observations is that in addition to impairing cell spreading or TGN maintenance, these mutants may be sequestering other interaction partners in cells, which may contribute to the severity in the phenotypes. This may be yet another reason for cellular phenotype heterogeneity. Nevertheless, it needs to be determined if patients carrying these mutants indeed have specific or more severe clinical manifestations of LS compared to others.

The heterogenous behavior of mutants within a given domain, creates yet another level of complexity when we try to establish a correlation between the genotype and cellular phenotypes of LS. For instance, though $Ocrl1^{V508D}$ exhibited all phosphatase domain-specific defects, the

phenotypes induced by this variant were milder in comparison to other mutants within the same domain.

Taking together the various aspects of heterogeneity the mutants presented with, we propose that even though Ocrl1's function is spatially segregated within the protein, we have demonstrated that mutations affecting these domains do not impact its function in the same manner. In addition to the domain affected by the mutation, we must consider

1. Effect of mutations on intrinsic properties of mutant Ocrl1 including stability, biochemical interactions and intracellular localization.
2. Mutations in *OCRL1* trigger diverse phenotypes, some of which are common to mutants across different domains, which some are unique to specific Ocrl1 domains.
3. Some phenotypes like Golgi apparatus fragmentation are exacerbated in the presence of mutant Ocrl1 when compared to having no Ocrl1.

Therefore, the impact of *OCRL1* mutations on LS cellular phenotypes is a composite of all the above factors. This is the first study to provide compelling evidence for heterogeneity in LS cellular phenotypes. It is however imperative to keep in mind that in how this links to LS patient symptom heterogeneity needs to be directly tested. And besides the vast cellular basis for heterogeneity, genetic modifiers as well as environmental factors may play a role in how these defects manifest as patient symptoms.

Materials and Methods

Reagents and constructs

All reagents were procured from Fisher Scientific (Fairlawn, NJ) or Sigma Aldrich (St. Louis, MO) unless stated otherwise. Antibodies used in this study are listed in Table II. Site-directed mutagenesis was performed using Quikchange Lightning mutagenesis kit (Agilent Technologies) and pEGFP-c1 hs*OCRL1* (wild-type, isoform b) as template to create the various *OCRL1* constructs used in this study. Plasmid constructs used in this study are listed in Table III.

Cells and culture conditions

Normal human proximal tubule epithelial (HK2) and human embryonic kidney epithelial 293T (HEK293T) cells were purchased from ATCC and cultured in DMEM, Streptomycin/Penicillin, 2mM L-Glutamine and 10% fetal bovine serum (FBS). Cells were maintained at 37 ºC in a 5% CO_2 incubator. *OCRL1*$^{-/-}$ (*OCRL* KO) HK2 and HEK293T cells were prepared by GenScript Inc. Piscataway, NJ, USA and maintained under identical conditions. Absence of Ocrl1 as well LS-specific phenotypes including cell spreading and ciliogenesis defects were previously validated in the KO cell lines (42, 57).

Preparation of stable cell lines

HK2 cells (and HK2 KO) have been immortalized using a plasmid encoding SV40 large T antigen than confers it resistance to G418 (ATCC). However, all plasmids encoding *hsOCRL1* utilize G418 to provide mammalian selection. To overcome the inherent G418 resistance HK2 KO cells exhibit, we co-transfected our plasmid of interest (encoding Ocrl1^{WT} or Ocrl1 mutants) with pTre2Hyg-6XHis vector (uses Hygromycin for mammalian selection) which was used to select for cells that stably integrated plasmid. Plasmids were transfected at 4:1 DNA ratio (1.6ug plasmid of interest: 0.4ug selection plasmid). This approach was used to ensure that a fraction of cells

expressing our plasmid will also express the selectable marker carrying plasmid. 24h after transfection, cells were treated with complete media containing 100ug/ml Hygromycin (Bruce et al.) Media was replaced every 48h with fresh media containing antibiotic. By 7 days of selection, we observed cells with stably integrated plasmid of interest (by observing GFP fluorescence). Within 2-3 weeks, colonies of stable clones (3/Ocrl1 variant) were identified and isolated using sterile cloning discs. These clones were sub-cultured over multiple passages and TGN localization of Ocrl1 was confirmed by indirect immunofluorescence.

Transfections

Plasmids encoding different Ocrl1 mutants were transfected using Fugene 6 reagent (Promega) according to manufacturer's instructions. Briefly, 4ul of Fugene 6 reagent was added dropwise to 200ul of DMEM media (free of serum and antibiotics) and incubated for 5min at room temperature. Then, 1ug of plasmid DNA was added to this mixture dropwise and incubated for 15min at room temperature to allow complex formation. This mixture was added dropwise to freshly plated cells. Cells were incubated with this mixture for 18h to allow for plasmid uptake and expression following which they were used for different assays.

Cell spreading assays

Cells were transfected as described above and grown in complete media upto 18h. Cell confluency was maintained at ~50% to ensure single cell suspensions were obtained prior to spreading assays. 18h post transfection, the cells were lifted with 20mM EDTA (in 1X PBS), pelleted at 100xg for 5min and resuspended in complete media. Cell suspensions were then set in a rotator for 1 hour before seeding them on 10ug/ml fibronectin-coated coverslips for 30min, undisturbed, to allow attachment and spreading. At 30min, coverslips were gently washed using 1X PBS and fixed in 4% formaldehyde for 10min at room temperature. Cells were stained with

rhodamine–phalloidin (used at 1:200) and imaged by epifluorescence microscopy. At least 40 cells were analyzed per experiment. The magic wand tool in ImageJ software was used to trace the cell boundaries and determine cell areas and perimeter.

In every experiment, spreading area of cells expressing Ocrl1 mutants was normalized to the median area calculated in Ocrl1^{WT}-expressing for that respective experiment. Histograms were constructed from the normalized spreading area values and Kolmogorov-Smirnov (KS) test was performed to determine statistical significance.

Ciliogenesis assays

Cells were seeded (in complete media) on glass cover slips coated with poly-D-lysine and transfected as described above. Confluency of cells was maintained in such a way that it did not exceed 50% at the time of ciliogenesis. 18h after transfection, the media was replaced by 0.1% serum DMEM (starvation media) for another 24h to induce ciliogenesis. Cells were washed with 1X PBS, fixed in 4% formaldehyde–PBS for 10min. Indirect immunofluorescence was performed using antibodies against acetylated tubulin antibody (to label cilium) and pericentrin-2 (PC-2; to label centriole) (refer to Table I). 20 random fields, comprising of at least 50 cells were imaged for every experiment and repeated at least thrice.

From all the transfected cells imaged, the fraction of Ocrl1 mutant-transfected cells forming a cilium was calculated. This was normalized to the fraction of cilia produced by Ocrl1^{WT}-expressing cells from the respective experiment. The upper limit of fraction of ciliated cells was 1 (represented by HEK293T KO cells expressing Ocrl1^{WT}) while the lower limit of fraction of ciliated cell was 0.7 (HEK293T KO cells expressing Ocrl1^{GFP}). Though we observed variability between experiments, individual experiments were statistically significant.

Indirect immunofluorescence and fluorescence microscopy

In all immunofluorescence procedures, antibodies were diluted in DMEM media containing 10% FBS (blocking agent) and 0.1% saponin (permeabilizing agent). Primary antibodies were incubated for 1h at room temperature, washed 2X with PBS. Fluorescent molecule-conjugated secondary antibodies were incubated with cells for 45min in the dark, washed 2X with PBS. Cells were then stained using DAPI to label the nucleus and mounted on pre-cleaned glass slides using Aqua-PolyMount reagent (Polysciences). Following indirect immunofluorescence, coverslips were imaged with constant fluorescence exposure times using a 40X objective on Zeiss Axiovert inverted microscope. Random fields were imaged to cover the entire coverslip. Exposure times were maintained consistent for all independent experiments.

Protein purification

The PH and phosphatase domain of wild-type hsOcrl1 (1-563 amino acids) was cloned in a pGEX-4T1 plasmid (Clontech) that contains an N-terminus glutathione S-transferase (GST) tag. Using site directed mutagenesis, missense mutations H524R, D451G and V508D were introduced. Plasmids were transformed in Rosetta (DE3) competent cells. Bacterial cultures were grown overnight at 37°C, in LB medium supplemented with 2.5% glucose, 1X ampicillin, and 1X chloramphenicol. The following day, cultures were expanded in super broth media containing 1X ampicillin and 1X chloramphenicol for 3 hours at 37 °C. Then, cultures were supplemented with 5% glycerol and 0.1 mM IPTG and incubated for 5 hours at 30 °C.

Cells were harvested by centrifugation (3,000 x g, 10 min), and pellets were stored at -80 °C until use. Cells were lysed in lysis buffer containing 200 mM Tris pH 7.4, 10% glycerol, 01.% Tween 20, complete EDTA-free protease inhibitor, 1 mg/ml lysozyme was added to resuspend prepared cell pellets. Cells were disrupted by sonication at 50% power for 3 sets of 33 pulses with 30 second breaks in between pulses. Cell debris was removed via centrifugation at 21,500 x g, 30

min, 4 °C. The supernatant was transferred to tubes containing glutathione resin (Pierce) and incubated at room temperature on a shaker (12 rpm) for 2 hours. Beads were washed 4 times with lysis buffer (w/o protease inhibitor and lysozyme). Then, 100 mM glutathione (pH 8.0) was added to the tubes containing supernatant and incubated at room temperature on a shaker (12 rpm) for 2 hours to elute the protein. Supernatant (after centrifugation at 1,000 x g for 2 min) was loaded onto desalting columns (Thermo Scientific, Zeba, 89891) and centrifuged (1,000 x g, 2 min, acceleration: 5) and purified protein was obtained. Protein concentration was estimated using NanoDrop 1000 (ThermoFisher) and was used immediately for malachite green phosphatase assays.

Malachite green phosphatase assays

For 5' phosphatase activity assays, the malachite green phosphate assay kit (Sigma-Aldrich, MAK307) was used. Briefly, in a 384-well plate, 10 µl of 2µM of purified Ocrl1 (wildtype and mutant) was incubated with drug or vehicle for one hour at room temperature, to obtain a final enzyme concentration of 1uM. After treatment,10 µl of 50 µM PI(4,5)P2 diC8 (Echelon Biosciences, P-4508) was added to wells and incubated for 5 minutes at room temperature in the same buffer as the purified phosphatases, containing 200 mM Tris, pH 7.4. To stop enzyme reaction, 20 µl of 0.25X malachite green reagent was added to the reaction wells. After 20 minutes of color development, absorbance was measured at 620 nm. A standard phosphate curve was prepared (as per manufacturer's instructions) in the enzyme buffer solution to determine the amount of free phosphate released by the enzyme variants tested. Experiments were repeated at least thrice and each condition was tested in triplicates. Student's t-test was used to determine statistical significance.

Statistical analysis

Statistical significance of differences between spreading-distribution histograms were analyzed using the Kolmogorov-Smirnov (KS) test. The student's t-test was used to evaluate the significance of differences of normally distributed samples (ex. for ciliogenesis experiments), while the Wilcoxon's test was employed when samples were non-normally distributed (Quantification of Golgi apparatus fragmentation and PC2 colocalization). For all comparisons involving Ocrl1^{WT} and Ocrl1 mutants, the Bonferroni's correction for multiple comparisons was performed whenever applicable [$\alpha C=p/n$; n being the number of comparisons].

After carefully analyzing each data set distribution the most appropriate representation of data in each case was adopted. These representations included histograms and box plots as they allow to thoroughly examine the data distribution (58). When the data presented a normal distribution, a bar graph with standard deviations was used to represent the data.

Table I

Mutation	Domain affected
S256N	5’ phosphatase
D451G	5’ phosphatase
V508D	5’ phosphatase
H524R	5’ phosphatase
V577E	ASH-RhoGAP
F668V	ASH-RhoGAP
I768N	ASH-RhoGAP

Table II: Antibodies used in this study			
Antigen	**Host**	**Source**	**Dilution used and application**
Acetylated-Tubulin	Mouse	Sigma Aldrich (6-11B-1)	1:1000 (IIF)
Pericentrin-2 (PC-2)	Rabbit	Abcam (ab4448)	1:300 (IIF)
TGN46	Rabbit	Thermo Fisher (PA5-23068)	1:400 (IIF)
IIF: Indirect Immuno-Fluorescence			

Table III: Plasmids used in this study			
Construct name	**Species**	**Vector**	**Source**
GFP		pEGFP-c1	Clontech
Ocrl1^{WT}	*Homo sapiens* (isoform b)	pEGFP-c1	Coon et al. 2009
Ocrl1^{S256N}	*Homo sapiens* (isoform b)	pEGFP-c1	This study
Ocrl1^{D451G}	*Homo sapiens* (isoform b)	pEGFP-c1	Coon et al. 2009
Ocrl1^{V508D}	*Homo sapiens* (isoform b)	pEGFP-c1	This study
Ocrl1^{H524R}	*Homo sapiens* (isoform b)	pEGFP-c1	This study
Ocrl1^{V577E}	*Homo sapiens* (isoform b)	pEGFP-c1	This study
Ocrl1^{F668V}	*Homo sapiens* (isoform b)	pEGFP-c1	This study
Ocrl1^{I768N}	*Homo sapiens* (isoform b)	pEGFP-c1	This study
Ocrl1$^{\Delta PH}$	*Homo sapiens* (isoform b)	pEGFP-c1	This study
pTRe2HygZ		pTRe2HygZ	Clontech

Figure legends

Fig. 1 LS mutations tested in this study mapped on the different Ocrl1 domains they affect (A). Representation of the proposed alternative Ocrl1 transcript (B). Legend: PH: Pleckstrin homology, IPPc: Inositol polyphosphate phosphatase, catalytic, ASH: ASPM-SPD- 2-Hydin RhoGAP: RhoGTPase Activating Protein.

Fig. 2 Ocrl1 patient variants differentially affect cell spreading. HEK293T KO cells were transfected with Ocrl1^{WT}, Ocrl1$^{\Delta PH}$ (A) phosphatase domain mutants (B) or ASH-RhoGAP domain mutants (C) and allowed to attach and spread on fibronectin-coated surfaces (See *Materials and Methods*). Median spreading areas of cells expressing mutants were normalized with respect to Ocrl1^{WT} of corresponding experiments. Histograms are from a single representative experiment, n=40 cells. Experiments were repeated at least 3 times, with a total n=120-150 cells. Example of stained cells representative of the high frequency groups within each histogram. Scale bar: 10µm. A: **p<0.05, B: **p<(0.05/4=0.0125), N.S not significant C: **p<(0.05/3=0.0167) (Bonferroni correction) by the KS test, *p<0.05. Arrows indicate punctate perinuclear structure produced by ASH-RhoGAP mutants (C).

Fig. 3 Ocrl1 patient variants differentially affect ciliogenesis. HEK293T KO cells were transfected with different Ocrl1^{WT} or Ocrl1$^{\Delta PH}$, phosphatase domain mutants (A) or ASH-RhoGAP domain mutants (B) and ciliogenesis assays were performed (see *Materials and Methods*). 20 random fields with at least 50 cells were imaged and fraction of transfected cells with cilia were calculated. This number was normalized to fraction of Ocrl1^{WT}-expressing cells forming cilia. Each experiment was repeated at least thrice (n=120-150 cells). Scale bar: 10µm. A: **p<(0.05/5=0.01), B: **p<(0.05/3=0.0167) (Bonferroni correction) by the Student's t-test, *p<0.05. Green reference line represents fraction of Ocrl1^{WT} expressing cells making cilia. ***p<0.0001.

Fig. 4 Truncation of Ocrl1 PH domain results in nuclear mislocalization of variant. HK2 KO cells transiently expressing GFP (top panel), Ocrl1^{WT} (middle panel) or Ocrl1$^{\Delta PH}$ and immunostained for TGN (see *Materials and Methods*). Yellow arrows indicate Ocrl1$^{\Delta PH}$ enrichment in the nuclear compartment. Scale bar: 10µm.

Fig. 5 Phosphatase domain mutants produce Golgi apparatus fragmentation. A: HK2 KO cells transiently transfected with Ocrl1^{WT} (top panel) or Ocrl1^{D451G} (second panel) or Ocrl1^{V508D} (third panel) or Ocrl1^{S256N} (bottom panel) and immunostained for TGN. Yellow highlighted region in merged images corresponding to the TGN area which was scaled to 4X (inset images) to better visualize Golgi apparatus fragmentation. Yellow arrows indicate fragmented TGN puncta that lack Ocrl1. White arrows indicate dispersed mutant Ocrl1 lacking colocalization. Scale bar: 10µm. B: At least 40 transfected cells were imaged randomly, per experiment and area occupied by TGN was quantified (See *Materials and Methods*). Each experiment was repeated at least thrice with total n=120-150 cells/group. **p<(0.05/2=0.025) (Bonferroni correction) by the Wilcoxon test. C: Golgi apparatus fragmentation plotted as a function of total fluorescence intensity of Ocrl1 (WT/patient variant) transfected in HK2 KO cells. D: HK2 KO cells stably expressing Ocrl1^{WT} or Ocrl1^{H524R} or Ocrl1^{D451G} (see *Materials and Methods*) were prepared. All cells stably expressing Ocrl1 variants were imaged and TGN area was quantified

(see *Materials and Methods*). Scale bar: 10µm. E: Golgi apparatus fragmentation determined as a function of total cell area. **p<(0.05/2=0.025) (Bonferroni correction) by the KS test.

Fig. 6 ASH-RhoGAP domain mutants exhibit enrichment or accumulation at the centriole under steady state (serum-fed) conditions. A: HK2 KO cells transiently expressing Ocrl1^{WT} or ASH-RhoGAP mutants (left panel) immunostained for PC-2 (centriole marker; middle panel) (see *Materials and Methods*). Yellow arrows indicate Ocrl1 at PC-2 labeled structures. B: Transfected cells were randomly imaged from at least 25 fields containing at least 40 cells. Cells with Ocrl1 colocalization to PC-2 were scored and fraction of cells exhibiting colocalization in a field was determined. **p<(0.05/3=0.0167) (Bonferroni correction) by the Wilcoxon test; box plot of a representative experiment. Red reference line indicates enrichment observed in GFP-transfected cells. C: Correlation of levels of expression of Ocrl1 patient variants with PC2 colocalization (left panel) or aggregate formation (right panel). D: HK2 KO cells transiently expressing Ocrl1^{V577E} (top panel) or Ocrl1^{I768N} exhibiting protein aggregation. E: HK2 KO cells stably expressing Ocrl1^{I768N} immunostained for PC-2 (centriole marker) (see *Materials and Methods*). Yellow highlighted region in merged images corresponding to the perinuclear region which was scaled to 2X (inset images) to better visualize Ocrl1 and PC2 colocalization. Yellow arrows indicate Ocrl1 at PC-2 labeled structures. Scale bar: 10µm.

Fig. 7 A: Mapping of all LS causing *OCRL1* missense mutations in the phosphatase domain, inset highlights location of mutations H524R, D451G and V508D. B: Molecular dynamics prediction of the effect of D451G mutation on Ocrl1 phosphatase domain structure. Ocrl1 phosphatase domain crystal structure (PDB ID: 4CMN) was used to run molecular dynamics simulations. WT (left) domain represented by stick model; blue color represents catalytic residues. Mutation of residue 451 Asp (D) to Gly (G) in this model (right, represented by orange shape fill) resulted in change in the position of catalytic blue residues (listed in white boxes) and acquired new position in red, resulting in overall conformation changes within the phosphatase domain.

Fig. 8 Ocrl1 phosphatase domain mutants are impaired for 5' phosphatase activity
Bacterially expressed GST-tagged Ocrl1 (amino acids 1-563; encoding PH and phosphatase domain); WT (top panel left) and the different phosphatase mutants were purified (See *Materials and Methods*). In vitro Malachite green phosphatase assays were performed (See *Materials and Methods*). Standard curve for each experiment was prepared and free phosphate generated by Ocrl1 variants was calculated. Experiments were done with constant enzyme and substrate concentration, only varying the incubation times of enzyme and substrate (X-axis). All experiments were done in triplicates and repeated at least thrice. **p<(0.05/3=0.0167) (Bonferroni correction) by Student t-test.

Fig. 1

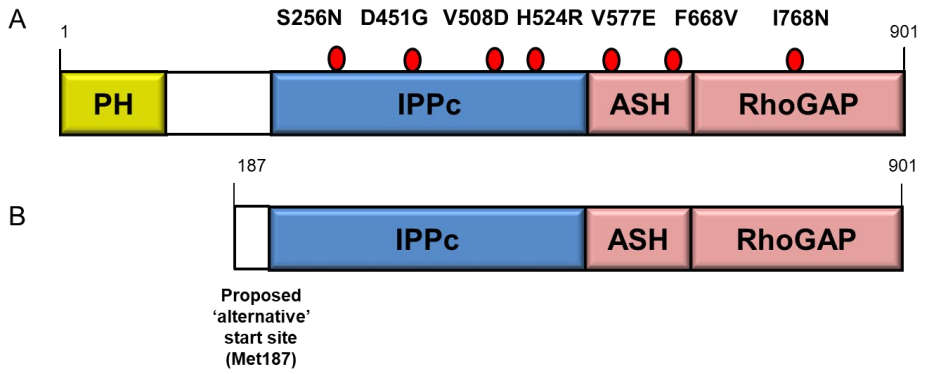

Fig. 2

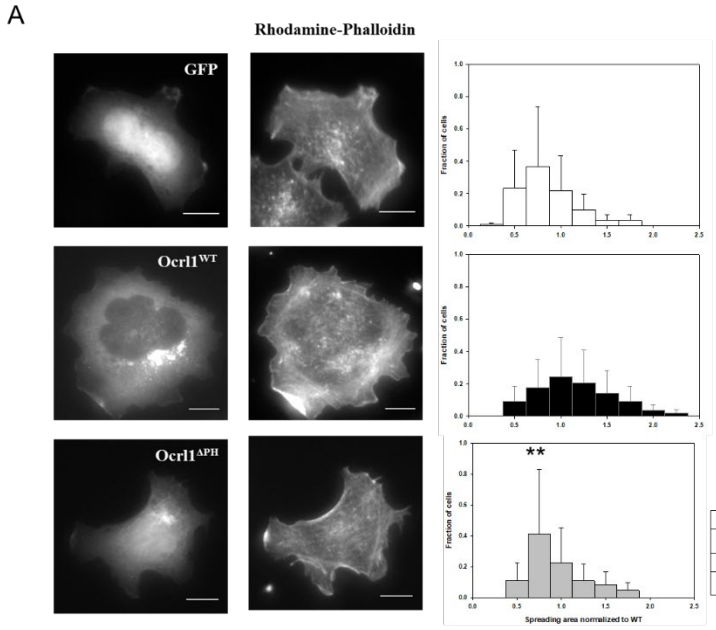

KS test		
Variant	Median	p value
WT	1	
ΔPH	0.7201	0

B

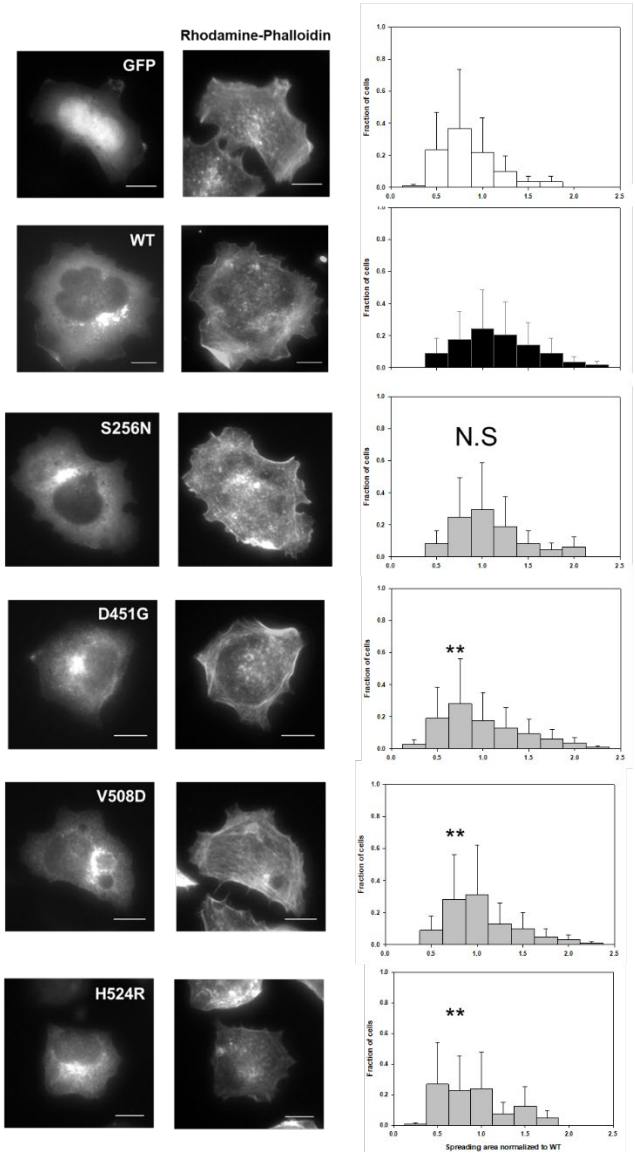

KS test		
Variant	Median	p value
WT	1	
S256N	0.9005	0.307
D451G	0.8007	0.003
V508D	0.8893	0.011
H524R	0.7268	0

C

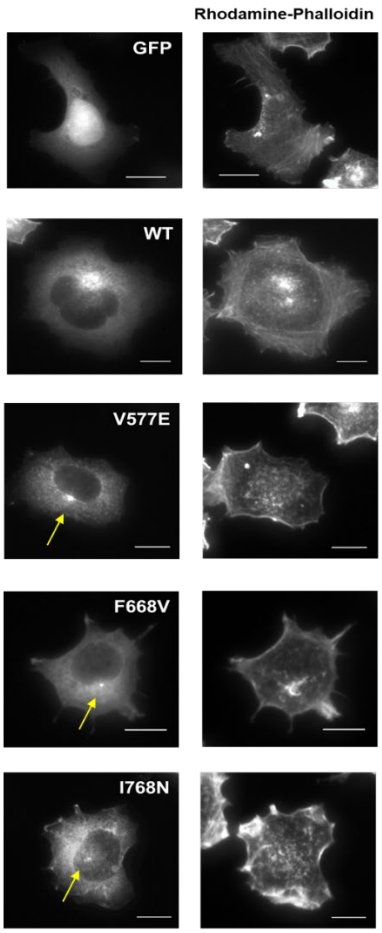

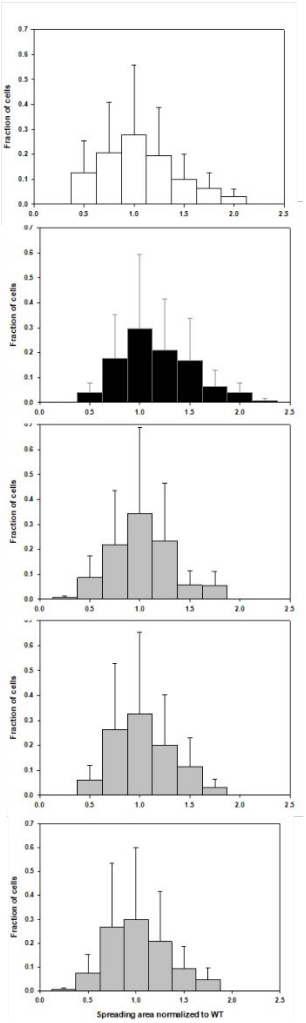

KS test		
Variant	**Median**	**p value**
WT	1	
V577E	0.8814	0.017
F668V	0.8872	0.054
I768N	0.8581	0.034

Fig. 3

A

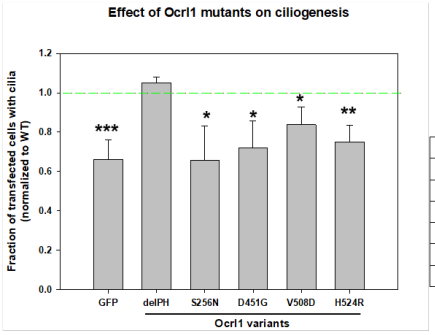

Unpaired Student's t-test	
Variant	p value
WT	
S256N	0.0257
D451G	0.0257
V508D	0.037
H524R	0.0056

B

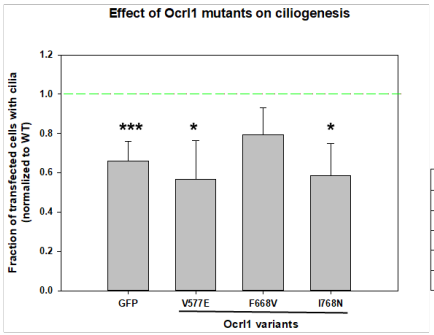

Unpaired Student's t-test	
Variant	p value
WT	
V577E	0.0189
F668V	0.0602
I768N	0.0113

Fig. 4

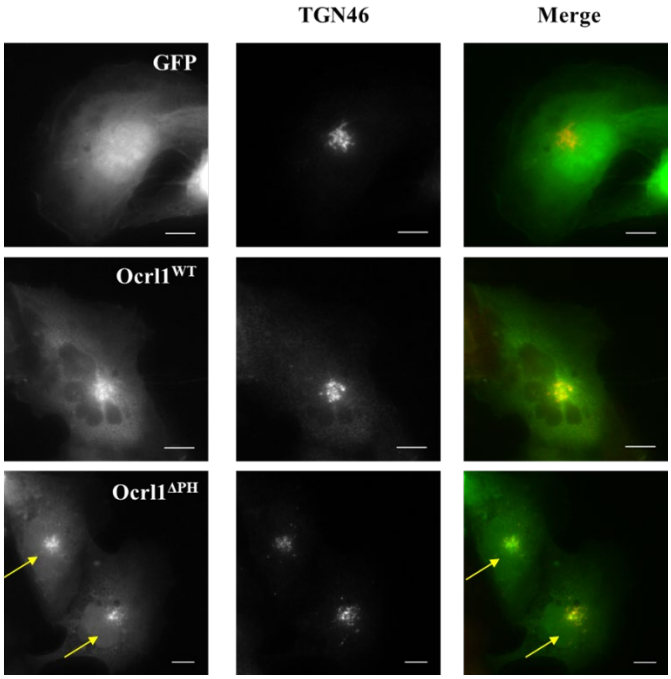

Fig. 5

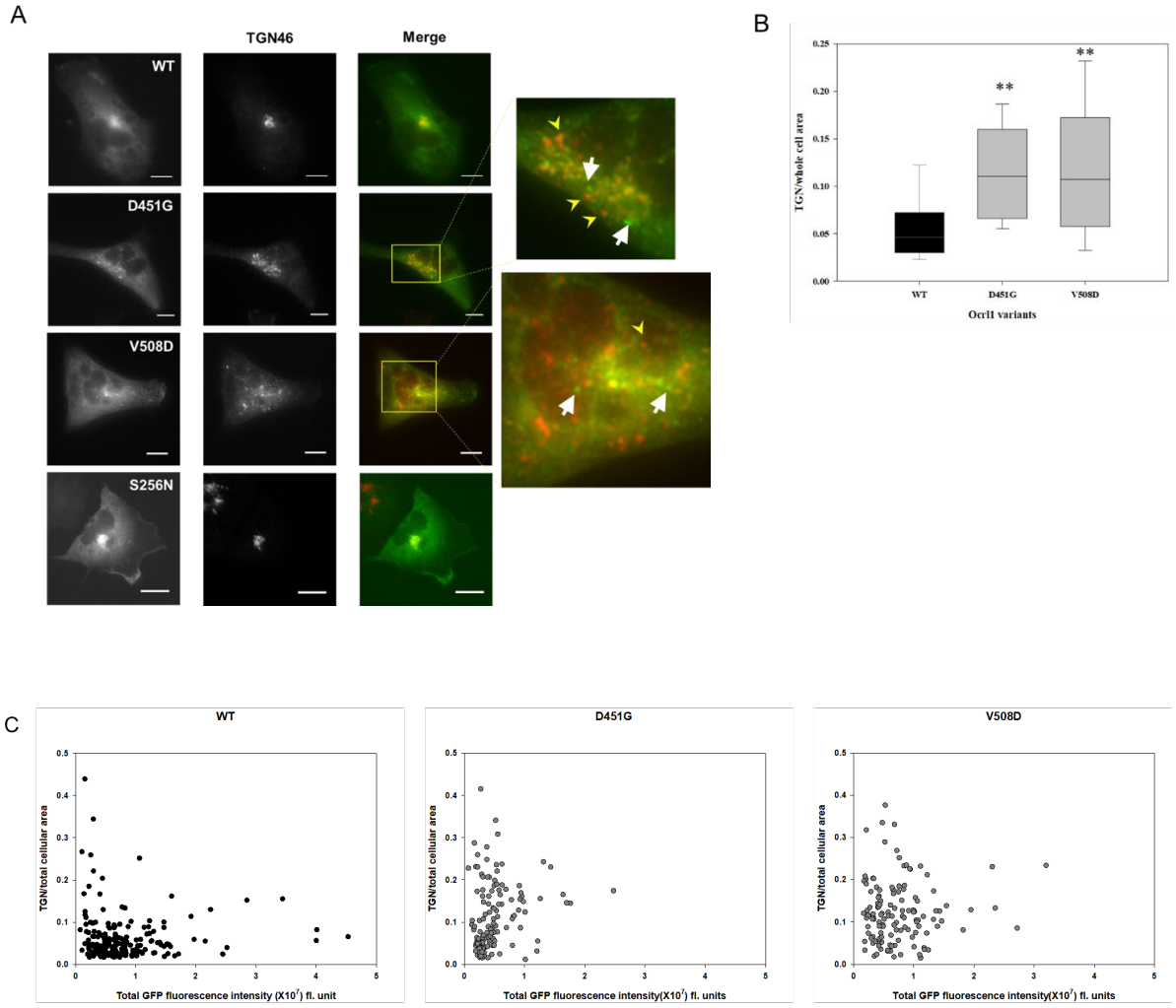
A
TGN46
Merge
WT
D451G
V508D
S256N
B
TGN/whole cell area
0.25
0.20
0.15
0.10
0.05
0.00
**
**
WT
D451G
V508D
OcrII variants
C
WT
D451G
V508D
TGN/total cellular area
Total GFP fluorescence intensity (X10^7) fl. unit
Total GFP fluorescence intensity(X10^7) fl. units

D

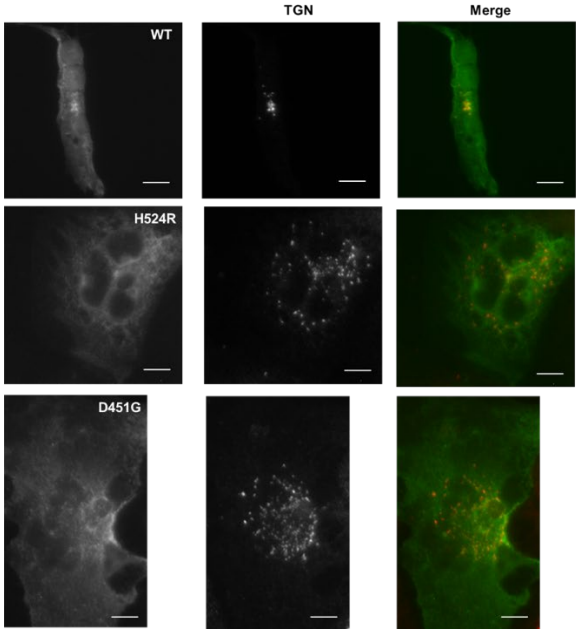
TGN
Merge
WT
H524R
D451G

E

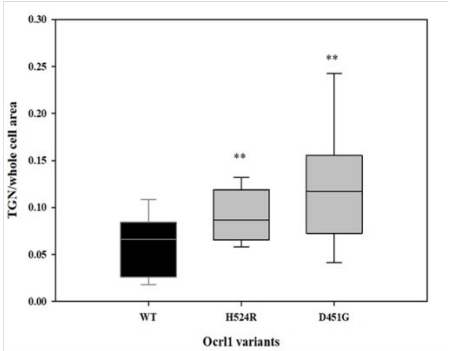
TGN/whole cell area
0.30
0.25
0.20
0.15
0.10
0.05
0.00
**
**
WT
H524R
D451G
Ocrl1 variants

Fig. 6

A

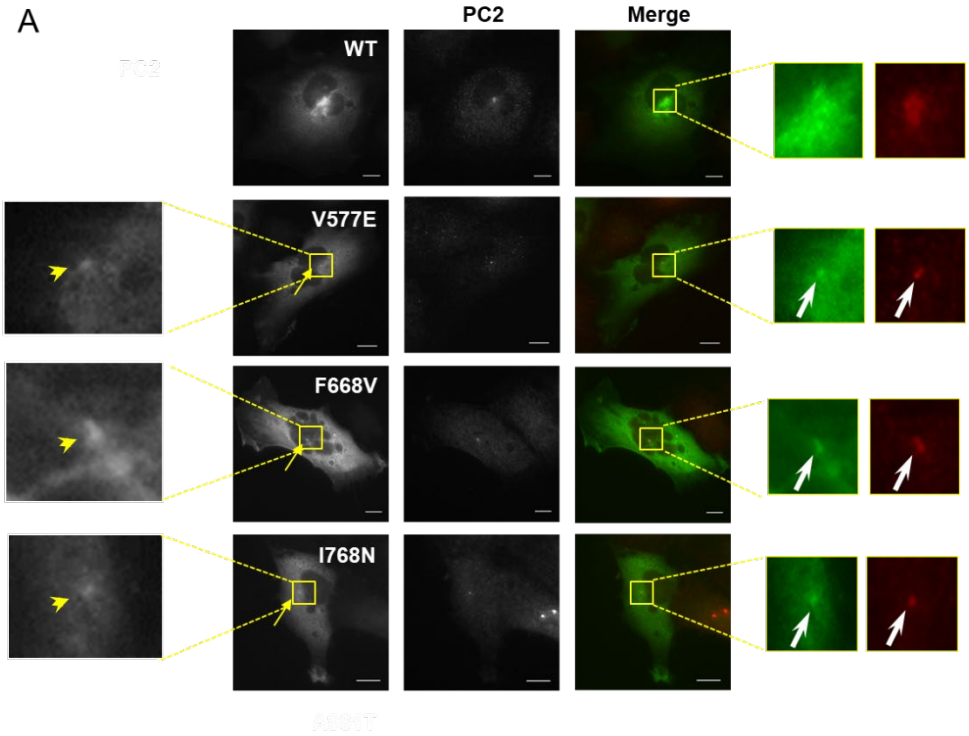
PC2
Merge
WT
V577E
F668V
I768N

B

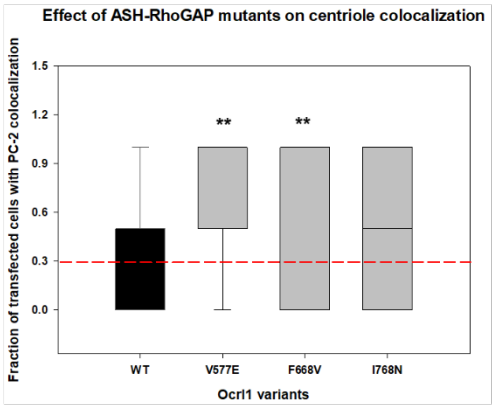
Effect of ASH-RhoGAP mutants on centriole colocalization
Fraction of transfected cells with PC-2 colocalization
1.5
1.2
0.9
0.6
0.3
0.0
**
**
WT
V577E
F668V
I768N
Ocrl1 variants

C

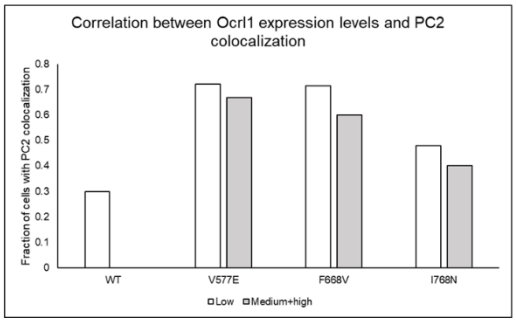
Correlation between Ocrl1 expression levels and PC2 colocalization
Fraction of cells with PC2 colocalization
0.8
0.7
0.6
0.5
0.4
0.3
0.2
0.1
0
WT
V577E
F668V
I768N
Low
Medium+high

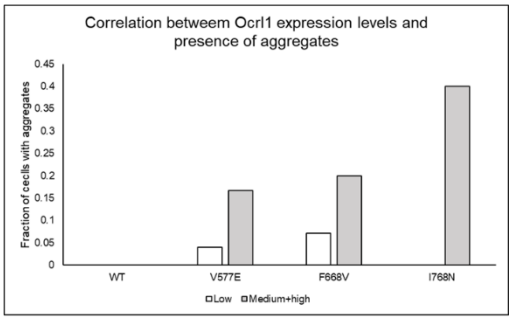
Correlation betweem Ocrl1 expression levels and presence of aggregates
Fraction of cecls with aggregates
0.45
0.4
0.35
0.3
0.25
0.2
0.15
0.1
0.05
0
WT
V577E
F668V
I768N
Low
Medium+high

D

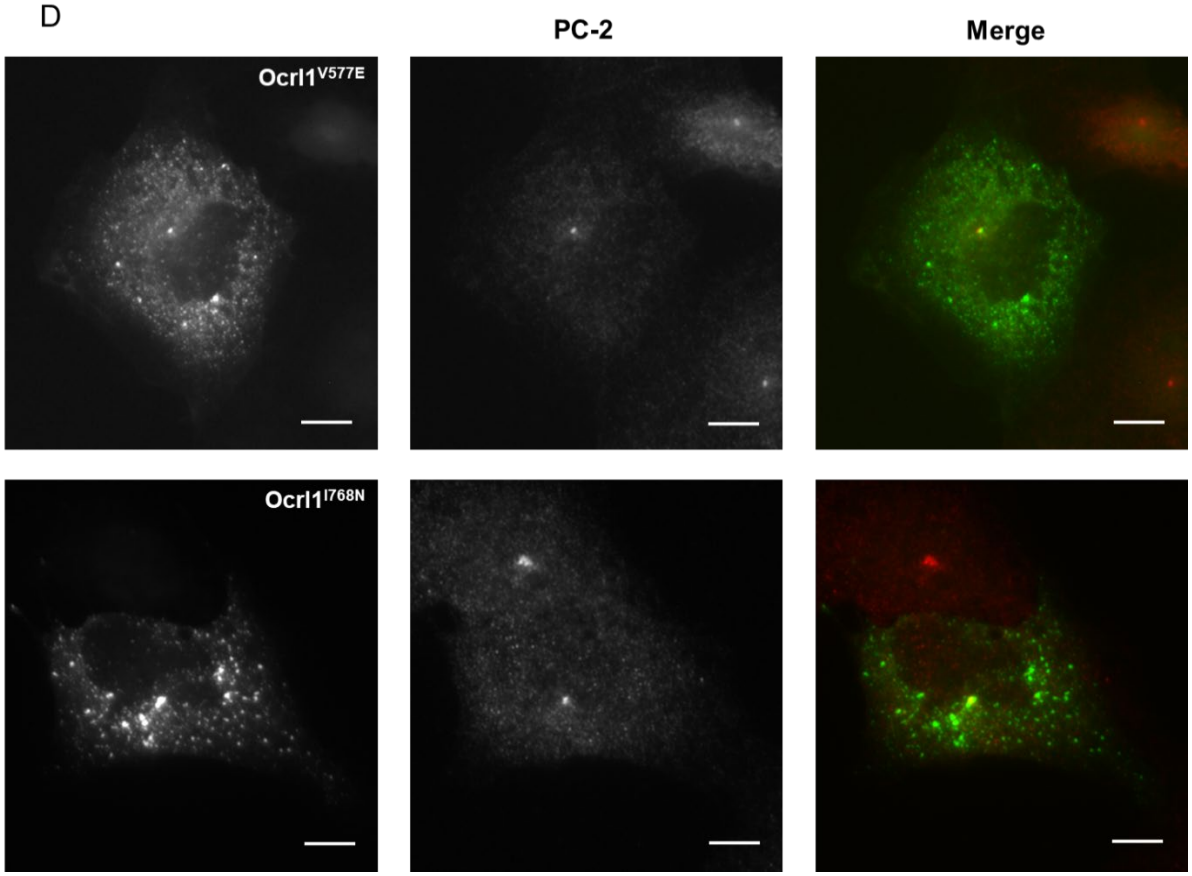

E

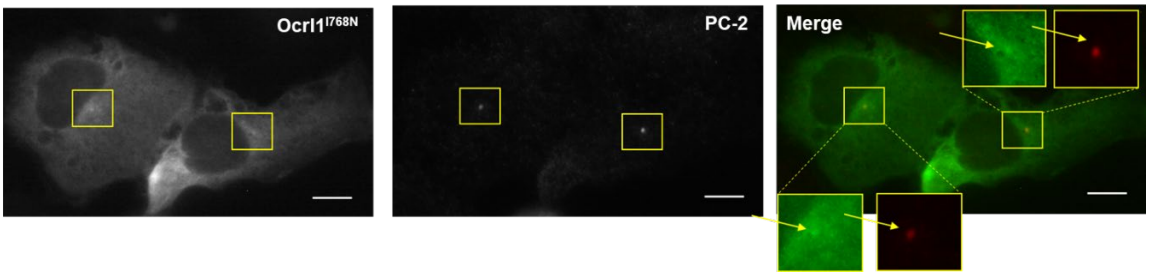

Fig. 7

A

```
        250       260       270       280       290       300
          |         |         |         |         |         |
RFFVGTWNVNGQSPDSGLEPWLNCDPNPPDIYCIGFQELDLSTEAFFYFESVKEQEWSMA
 S  E C G      N    C          NH T SR P                  C I
                                D     E

        310       320       330       340       350       360
          |         |         |         |         |         |
VERGLHSKAKYKKVQLVRLVGMMLLIFARKDQCRYIRDIATETVGTGIMGKMGNKGGVAV
                  H  E      P     P  C                  DE
                  C                                     V

        370       380       390       400       410       420
          |         |         |         |         |         |
RFVFHNTTFCIVNSHLAAHVEDFERRNQDYKDICARMSFVVPNQTLPQLNIMKHEVVIWL
I          GYFY                  F                     R  D
           E PR
              T

        430       440       450       460       470       480
          |         |         |         |         |         |
GDLNYRLCMPDANEVKSLINKKDLQRLLKFDQLNIQRTQKKAFVDFNEGEIKFIPTYKYD
EN D      N                     N    PG     S    G      HI
                                G     P          K      S

        490       500       510       520       530       540
          |         |         |         |         |         |
SKTDRWDSSGKCRVPAWCDRILWRGTNVNQLNYRSHMELKTSDHKPVSALFHIGVKVVDE
         N     L GYAGS R E  D    C        RGRQLD     S
                   QHQ                     NQ T
                                           TY S
                                            D

        550       560
          |         |
RRYRKVFEDSVRIMDRMENDFLP
```

IPPc consensus motifs (Jefferson, et al. 1996, Whisstock, et al. 2000, Tsujishita, et al. 2001, Tresaugeus, et al. 2014, Mills, et al. 2016)

Lipid chain interacting motifs (Tresaugeus, 2014)

Residues in blue mutated in Lowe Syndrome (LS), change indicated by residues in red

IPPc- inositol polyphosphate phosphatase, catalytic

B

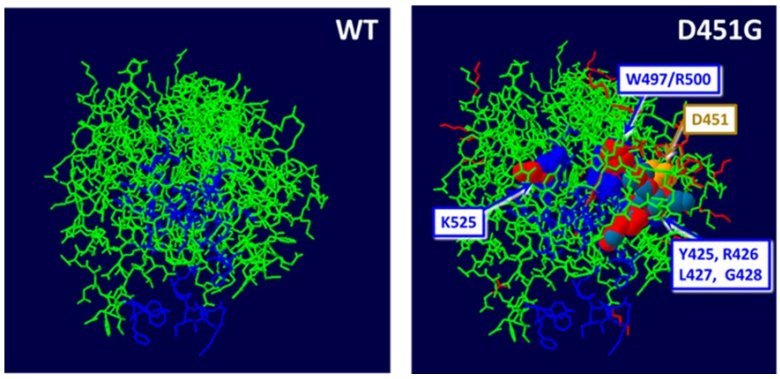
WT
D451G
W497/R500
D451
K525
Y425, R426
L427, G428

Fig. 8

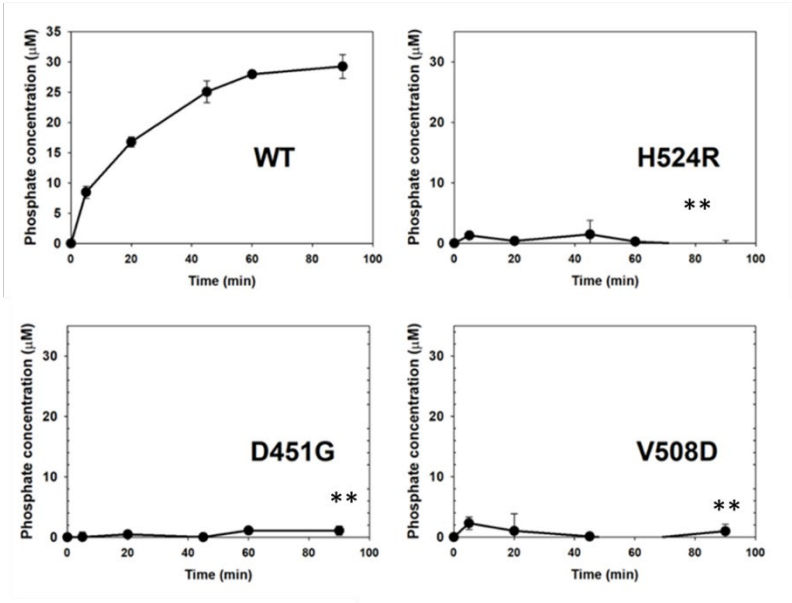
WT
H524R
D451G
V508D
Phosphate concentration (μM)
Time (min)
**

1 Attree, O., Olivos, I.M., Okabe, I., Bailey, L.C., Nelson, D.L., Lewis, R.A., McInnes, R.R. and Nussbaum, R.L. (1992) The Lowe's oculocerebrorenal syndrome gene encodes a protein highly homologous to inositol polyphosphate-5-phosphatase. *Nature*, **358**, 239-242.
2 Loi, M. (2006) Lowe syndrome. *Orphanet J Rare Dis*, **1**, 16.
3 LOWE, C.U., TERREY, M. and MacLACHLAN, E.A. (1952) Organic-aciduria, decreased renal ammonia production, hydrophthalmos, and mental retardation; a clinical entity. *AMA Am J Dis Child*, **83**, 164-184.
4 Bökenkamp, A. and Ludwig, M. (2016) The oculocerebrorenal syndrome of Lowe: an update. *Pediatr Nephrol*, **31**, 2201-2212.
5 Zhang, X., Jefferson, A.B., Auethavekiat, V. and Majerus, P.W. (1995) The protein deficient in Lowe syndrome is a phosphatidylinositol-4,5-bisphosphate 5-phosphatase. *Proc Natl Acad Sci U S A*, **92**, 4853-4856.
6 Suchy, S.F., Olivos-Glander, I.M. and Nussabaum, R.L. (1995) Lowe syndrome, a deficiency of phosphatidylinositol 4,5-bisphosphate 5-phosphatase in the Golgi apparatus. *Hum Mol Genet*, **4**, 2245-2250.
7 Dressman, M.A., Olivos-Glander, I.M., Nussbaum, R.L. and Suchy, S.F. (2000) Ocrl1, a PtdIns(4,5)P(2) 5-phosphatase, is localized to the trans-Golgi network of fibroblasts and epithelial cells. *J Histochem Cytochem*, **48**, 179-190.
8 Erdmann, K.S., Mao, Y., McCrea, H.J., Zoncu, R., Lee, S., Paradise, S., Modregger, J., Biemesderfer, D., Toomre, D. and De Camillil, P. (2007) A role of the Lowe syndrome protein OCRL in early steps of the endocytic pathway. *Developmental Cell*, **13**, 377-390.
9 Faucherre, A., Desbois, P., Nagano, F., Satre, V., Lunardi, J., Gacon, G. and Dorseuil, O. (2005) Lowe syndrome protein Ocrl1 is translocated to membrane ruffles upon Rac GTPase activation: a new perspective on Lowe syndrome pathophysiology. *Human Molecular Genetics*, **14**, 1441-1448.
10 Mao, Y., Balkin, D.M., Zoncu, R., Erdmann, K.S., Tomasini, L., Hu, F., Jin, M.M., Hodsdon, M.E. and De Camilli, P. (2009) A PH domain within OCRL bridges clathrin-mediated membrane trafficking to phosphoinositide metabolism. *Embo Journal*, **28**, 1831-1842.
11 Ponting, C.P. (2006) A novel domain suggests a ciliary function for ASPM, a brain size determining gene. *Bioinformatics*, **22**, 1031-1035.
12 Coon, B.G., Mukherjee, D., Hanna, C.B., Riese, D.J., II, Lowe, M. and Aguilar, R.C. (2009) Lowe syndrome patient fibroblasts display Ocrl1-specific cell migration defects that cannot be rescued by the homologous Inpp5b phosphatase. *Human Molecular Genetics*, **18**, 4478-4491.
13 Suchy, S.F. and Nussbaum, R.L. (2002) The deficiency of PIP2 5-phosphatase in Lowe syndrome affects actin polymerization. *American Journal of Human Genetics*, **71**.
14 Vicinanza, M., Di Campli, A., Polishchuk, E., Santoro, M., Di Tullio, G., Godi, A., Levtchenko, E., De Leo, M.G., Polishchuk, R., Sandoval, L. *et al.* (2011) OCRL controls trafficking through early endosomes via PtdIns4,5P(2)-dependent regulation of endosomal actin. *Embo Journal*, **30**, 4970-4985.
15 Coon, B.G., Hernandez, V., Madhivanan, K., Mukherjee, D., Hanna, C.B., Barinaga-Rementeria Ramirez, I., Lowe, M., Beales, P.L. and Aguilar, R.C. (2012) The Lowe syndrome protein OCRL1 is involved in primary cilia assembly. *Human molecular genetics*, **21**, 1835-1847.
16 Choudhury, R., Diao, A.P., Zhang, F., Eisenberg, E., Saint-Pol, A., Williams, C., Konstantakopoulos, A., Lucocq, J., Johannes, L., Rabouille, C. *et al.* (2005) Lowe syndrome protein OCRL1 interacts with clathrin and regulates protein trafficking between endosomes and the trans-Golgi network. *Molecular Biology of the Cell*, **16**, 3467-3479.
17 van Rahden, V.A., Brand, K., Najm, J., Heeren, J., Pfeffer, S.R., Braulke, T. and Kutsche, K. (2012) The 5-phosphatase OCRL mediates retrograde transport of the mannose 6-phosphate receptor by regulating a Rac1-cofilin signalling module. *Human Molecular Genetics*, **21**, 5019-5038.

18 Dambournet, D., Machicoane, M., Chesneau, L., Sachse, M., Rocancourt, M., El Marjou, A., Formstecher, E., Salomon, R., Goud, B. and Echard, A. (2011) Rab35 GTPase and OCRL phosphatase remodel lipids and F-actin for successful cytokinesis. *Nature Cell Biology*, **13**, 981-U245.
19 El Kadhi, K.B., Roubinet, C., Solinet, S., Emery, G. and Carreno, S. (2011) The Inositol 5-Phosphatase dOCRL Controls PI(4,5)P2 Homeostasis and Is Necessary for Cytokinesis. *Current Biology*, **21**, 1074-1079.
20 Noakes, C.J., Lee, G. and Lowe, M. (2011) The PH domain proteins IPIP27A and B link OCRL1 to receptor recycling in the endocytic pathway. *Molecular Biology of the Cell*, **22**, 606-623.
21 Bohdanowicz, M., Balkin, D.M., De Camilli, P. and Grinstein, S. (2012) Recruitment of OCRL and Inpp5B to phagosomes by Rab5 and APPL1 depletes phosphoinositides and attenuates Akt signaling. *Molecular Biology of the Cell*, **23**, 176-187.
22 Marion, S., Mazzolini, J., Herit, F., Bourdoncle, P., Kambou-Pene, N., Hailfinger, S., Sachse, M., Ruland, J., Benmerah, A., Echard, A. *et al.* (2012) The NF-kappa B Signaling Protein Bcl10 Regulates Actin Dynamics by Controlling AP1 and OCRL-Bearing Vesicles. *Developmental Cell*, **23**, 954-967.
23 Hichri, H., Rendu, J., Monnier, N., Coutton, C., Dorseuil, O., Poussou, R.V., Baujat, G., Blanchard, A., Nobili, F., Ranchin, B. *et al.* (2011) From Lowe Syndrome to Dent Disease: Correlations between Mutations of the OCRL1 Gene and Clinical and Biochemical Phenotypes. *Human Mutation*, **32**, 379-388.
24 Bexiga, M.G. and Simpson, J.C. (2013) Human diseases associated with form and function of the Golgi complex. *Int J Mol Sci*, **14**, 18670-18681.
25 Ayala, I. and Colanzi, A. (2017) Alterations of Golgi organization in Alzheimer's disease: A cause or a consequence? *Tissue Cell*, **49**, 133-140.
26 Martínez-Menárguez, J., Tomás, M., Martínez-Martínez, N. and Martínez-Alonso, E. (2019) Golgi Fragmentation in Neurodegenerative Diseases: Is There a Common Cause? *Cells*, **8**.
27 Utsch, B., Bökenkamp, A., Benz, M.R., Besbas, N., Dötsch, J., Franke, I., Fründ, S., Gok, F., Hoppe, B., Karle, S. *et al.* (2006) Novel OCRL1 mutations in patients with the phenotype of Dent disease. *Am J Kidney Dis*, **48**, 942.e941-914.
28 Shrimpton, A.E., Hoopes, R.R., Jr., Knohl, S.J., Hueber, P., Reed, A.A., Christie, P.T., Igarashi, T., Lee, P., Lehman, A., White, C. *et al.* (2009), In *Nephron Physiol*, Switzerland, Vol. 112, pp. p27-36.
29 Fan, J., Hu, Z., Zeng, L., Lu, W., Tang, X., Zhang, J. and Li, T. (2008) Golgi apparatus and neurodegenerative diseases. *Int J Dev Neurosci*, **26**, 523-534.
30 Caracci, M.O., Fuentealba, L.M. and Marzolo, M.P. (2019) Golgi Complex Dynamics and Its Implication in Prevalent Neurological Disorders. *Front Cell Dev Biol*, **7**, 75.
31 Whisstock, J.C., Romero, S., Gurung, R., Nandurkar, H., Ooms, L.M., Bottomley, S.P. and Mitchell, C.A. (2000) The inositol polyphosphate 5-phosphatases and the apurinic/apyrimidinic base excision repair endonucleases share a common mechanism for catalysis. *Journal of Biological Chemistry*, **275**, 37055-37061.
32 Tsujishita, Y., Guo, S.L., Stolz, L.E., York, J.D. and Hurley, J.H. (2001) Specificity determinants in phosphoinositide dephosphorylation: Crystal structure of an archetypal inositol polyphosphate 5-phosphatase. *Cell*, **105**, 379-389.
33 Tresaugues, L., Silvander, C., Flodin, S., Welin, M., Nyman, T., Graslund, S., Hammarstrom, M., Berglund, H. and Nordlund, P. (2014), In *Structure*. 2014 Elsevier Ltd, United States, Vol. 22, pp. 744-755.
34 Jefferson, A.B. and Majerus, P.W. (1996) Mutation of the conserved domains of two inositol polyphosphate 5-phosphatases. *Biochemistry*, **35**, 7890-7894.
35 Mills, S.J., Silvander, C., Cozier, G., Trésaugues, L., Nordlund, P. and Potter, B.V. (2016) Crystal Structures of Type-II Inositol Polyphosphate 5-Phosphatase INPP5B with Synthetic Inositol Polyphosphate Surrogates Reveal New Mechanistic Insights for the Inositol 5-Phosphatase Family. *Biochemistry*, **55**, 1384-1397.

36 Lin, T., Orrison, B.M., Leahey, A.M., Suchy, S.F., Bernard, D.J., Lewis, R.A. and Nussbaum, R.L. (1997) Spectrum of mutations in the OCRL1 gene in the Lowe oculocerebrorenal syndrome. *Am J Hum Genet*, **60**, 1384-1388.
37 Shrimpton, A.E., Hoopes, R.R., Jr., Knohl, S.J., Hueber, P., Reed, A.A.C., Christie, P.T., Igarashi, T., Lee, P., Lehman, A., White, C. *et al.* (2009) OCRL1 Mutations in Dent 2 Patients Suggest a Mechanism for Phenotypic Variability. *Nephron Physiology*, **112**, 27-36.
38 Pirruccello, M. and De Camilli, P. (2012) Inositol 5-phosphatases: insights from the Lowe syndrome protein OCRL. *Trends Biochem Sci*, **37**, 134-143.
39 Pirruccello, M., Swan, L.E., Folta-Stogniew, E. and De Camilli, P. (2011) Recognition of the F&H motif by the Lowe syndrome protein OCRL. *Nat Struct Mol Biol*, **18**, 789-795.
40 Rbaibi, Y., Cui, S., Mo, D., Carattino, M., Rohatgi, R., Satlin, L.M., Szalinski, C.M., Swanhart, L.M., Folsch, H., Hukriede, N.A. *et al.* (2012) OCRL1 Modulates Cilia Length in Renal Epithelial Cells. *Traffic*, **13**, 1295-1305.
41 Luo, N., West, C.C., Murga-Zamalloa, C.A., Sun, L., Anderson, R.M., Wells, C.D., Weinreb, R.N., Travers, J.B., Khanna, H. and Sun, Y. (2012) OCRL localizes to the primary cilium: a new role for cilia in Lowe syndrome. *Human Molecular Genetics*, **21**.
42 Madhivanan, K., Ramadesikan, S., Hsieh, W.C., Aguilar, M.C., Hanna, C.B., Bacallao, R.L. and Aguilar, R.C. (2020) Lowe syndrome patient cells display mTOR- and RhoGTPase-dependent phenotypes alleviated by rapamycin and statins. *Hum Mol Genet*.
43 Bothwell, S.P., Farber, L.W., Hoagland, A. and Nussbaum, R.L. (2010) Species-specific difference in expression and splice-site choice in Inpp5b, an inositol polyphosphate 5-phosphatase paralogous to the enzyme deficient in Lowe Syndrome. *Mammalian Genome*, **21**, 458-466.
44 Janne, P.A., Suchy, S.F., Bernard, D., MacDonald, M., Crawley, J., Grinberg, A., Wynshaw-Boris, A., Westphal, H. and Nussbaum, R.L. (1998) Functional overlap between murine Inpp5b and Ocrl1 may explain why deficiency of the murine ortholog for OCRL1 does not cause Lowe syndrome in mice. *Journal of Clinical Investigation*, **101**, 2042-2053.
45 Leahey, A.M., Charnas, L.R. and Nussbaum, R.L. (1993) Nonsense mutations in the OCRL-1 gene in patients with the oculocerebrorenal syndrome of Lowe. *Hum Mol Genet*, **2**, 461-463.
46 Hyvola, N., Diao, A., McKenzie, E., Skippen, A., Cockcroft, S. and Lowe, M. (2006) Membrane targeting and activation of the Lowe syndrome protein OCRL1 by rab GTPases. *Embo Journal*, **25**, 3750-3761.
47 Hagemann, N., Hou, X., Goody, R.S., Itzen, A. and Erdmann, K.S. (2012) Crystal structure of the Rab binding domain of OCRL1 in complex with Rab8 and functional implications of the OCRL1/Rab8 module for Lowe syndrome. *Small GTPases*, **3**, 107-110.
48 Hou, X., Hagemann, N., Schoebel, S., Blankenfeldt, W., Goody, R.S., Erdmann, K.S. and Itzen, A. (2011) A structural basis for Lowe syndrome caused by mutations in the Rab-binding domain of OCRL1. *Embo Journal*, **30**, 1659-1670.
49 McCrea, H.J., Paradise, S., Tomasini, L., Addis, M., Melis, M.A., De Matteis, M.A. and De Camilli, P. (2008) All known patient mutations in the ASH-RhoGAP domains of OCRL affect targeting and APPL1 binding. *Biochemical and Biophysical Research Communications*, **369**, 493-499.
50 Vora, S.M. and Phillips, B.T. (2016) The benefits of local depletion: The centrosome as a scaffold for ubiquitin-proteasome-mediated degradation. *Cell Cycle*, **15**, 2124-2134.
51 Park, J., Park, Y., Ryu, I., Choi, M.H., Lee, H.J., Oh, N., Kim, K., Kim, K.M., Choe, J., Lee, C. *et al.* (2017) Misfolded polypeptides are selectively recognized and transported toward aggresomes by a CED complex. *Nat Commun*, **8**, 15730.
52 Olzmann, J.A., Li, L. and Chin, L.S. (2008) Aggresome formation and neurodegenerative diseases: therapeutic implications. *Curr Med Chem*, **15**, 47-60.

53 Johnston, J.A., Ward, C.L. and Kopito, R.R. (1998) Aggresomes: a cellular response to misfolded proteins. *J Cell Biol*, **143**, 1883-1898.
54 Kopito, R.R. and Ron, D. (2000) Conformational disease. *Nat Cell Biol*, **2**, E207-209.
55 Kopito, R.R. (2000) Aggresomes, inclusion bodies and protein aggregation. *Trends Cell Biol*, **10**, 524-530.
56 Rubenstein, R.C., Egan, M.E. and Zeitlin, P.L. (1997) In vitro pharmacologic restoration of CFTR-mediated chloride transport with sodium 4-phenylbutyrate in cystic fibrosis epithelial cells containing delta F508-CFTR. *J Clin Invest*, **100**, 2457-2465.
57 Hsieh, W.C., Ramadesikan, S., Fekete, D. and Aguilar, R.C. (2018) Kidney-differentiated cells derived from Lowe Syndrome patient's iPSCs show ciliogenesis defects and Six2 retention at the Golgi complex. *PLoS One*, **13**, e0192635.
58 Weissgerber, T.L., Milic, N.M., Winham, S.J. and Garovic, V.D. (2015) Beyond bar and line graphs: time for a new data presentation paradigm. *PLoS Biol*, **13**, e1002128.